IEEE Photonics Journal
An IEEE Photonics Society Publication

Open Access

Comparison of Fiber-Based Gas Pressure Sensors Using Hollow-Core Photonic Crystal Fibers

Volume 13, Number 2, April 2021

Xuemei Yang
Yongqi Li
Songyang Zhang
Shun Wang
Shun Wu

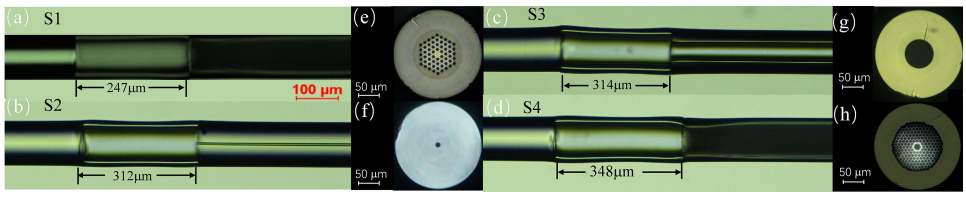

DOI: 10.1109/JPHOT.2021.3059925

Comparison of Fiber-Based Gas Pressure Sensors Using Hollow-Core Photonic Crystal Fibers

Xuemei Yang, Yongqi Li, Songyang Zhang, Shun Wang, and Shun Wu

Hubei Key Laboratory of Optical information and Pattern Recognition, Wuhan Institute of Technology, Wuhan 430205, China

DOI:10.1109/JPHOT.2021.3059925

Manuscript received January 11, 2021; revised February 10, 2021; accepted February 12, 2021. Date of publication February 17, 2021; date of current version March 12, 2021. This work was supported by the National Natural Science Foundation of China (NSFC) under Grant 61805182. Corresponding author: Shun Wu (e-mail: wushun@wit.edu.cn).

Abstract: A systematic comparison of fiber-based gas pressure sensors using different types of hollow-core photonic crystal fibers (PCFs) is conducted. The sensor was fabricated by splicing a segment of hollow-core silica capillary between a single mode fiber (SMF) and a hollow-core PCF. A Fabry-Perot (FP) cavity configuration is thus formed with the capillary tube as the sensing cavity, while the PCF acts as gas passage to the external environment. External pressure change would lead to the variation in the refractive index of air in the sensing cavity, resulting in a wavelength shift of the interference dips. The pressure sensitivity is measured to be around 4 nm/MPa, with a high linearity of 99.7% or above, regardless of the type of the PCFs we used as gas inlet. Among the four different PCFs, the large-mode-area (LMA) PCF shows the highest fringe contrast in the reflection spectrum. Modal analysis reveals that this is due to the high reflectivity caused by the solid core of LMA-PCF. Our experimental results also indicate that the length of the sensing cavity, as well as the offset fusion splice will influence the fringe contrast. The sensor has potential application in gas pressure sensing for advantages of high sensitivity, compact size and ease of fabrication.

Index Terms: Gas pressure sensor, hollow-core photonic crystal fiber.

1. Introduction

In recent years, photonic crystal fibers (PCF) have attracted much attention due to its unique microstructure with low transmission loss, characteristics of high birefringence, and highly flexible design. PCF can be classified into two categories depending on whether they have hollow hole structure: all-solid state PCF [1] and hollow-core PCFs [2]–[9]. The latter can be filled with liquids [2], [10], crystal liquids [11], glycerin [12], metal [13] or gases [5], [9], [14], [15] and thus is widely used in various fiber sensors. For pressure sensing, the sensing element is required to be accessible to the external environment to sense the pressure change. Hollow-core PCF thus becomes a good candidate, which can be used to form the sensing cavity [3], [6], [7], [16]–[18] in a Fabry-Perot (FP) cavity configuration. Compared to FPI-based pressure sensors with solid PCFs, FPIs with air-cavity have additional advantage of low temperature cross-sensitivity [15]. They can potentially work in high-temperature. Since pressure sensors require direct connection to

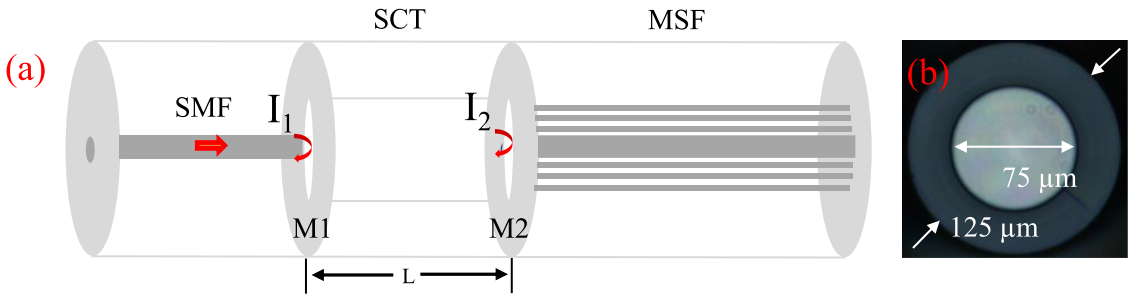

Fig. 1. (a) The schematic diagram of the proposed pressure sensor using silica capillary and micro hole structure fiber. (b) the side view of the cross section of 75 μm capillary tube.

the external environment, many researchers perform micromachining techniques, such as drilling hole on PCF utilizing femtosecond laser [6], [7] to allow gas flows in and out of the fiber. However, these sensors generally have the common disadvantages of a complicated manufacturing process and high cost.

As an alternative solution for creating gas inlets [2], [6], [16], [19], hollow-core PCFs serving as a gas inlet can also be useful. However, there are in general two challenges. The first challenge is that if both the sensing cavity and gas inlet are PCFs in a cascaded FP cavity configuration, it is difficult to splice two PCFs together without causing high loss [17], [18]. Another challenge is that the contrast ratio of the interference spectrum is small due to the low reflectivity of the second interface between the two PCFs [14]. So the selection of PCF is important. [20] He *et al.* proposed a FPI interferometer pressure sensor scheme in which a capillary tube acts as the sensing cavity and a second capillary tube with a smaller air hole diameter as the gas inlet, the contrast ratio of the interference fringes is as low as 1.5 to 3 dB. Most studies in the field of pressure sensing based on Fabry-Perot interferometers using PCFs have only focused on the configurations or high sensitivities. Unfortunately, the effect of various types of micro-structure fibers on the interference spectrum has not been detailed investigated to our best knowledge.

In this paper, we compare four fiber-based gas pressure sensors with Fabry-Perot cavity configuration utilizing different types of hollow-core PCFs. A silica capillary tube with 75 μm air hole in diameter forms the sensing cavity while four different types of PCFs serve as the gas inlet. The pressure sensitivity of the four sensors shows similar behavior, which is about 4 nm/MPa. This result is consistent with the calculated sensitivity by the interference model under two-beam approximation. Among the four PCFs, the interference fringes of the large-mode-are (LMA) a PCF has the highest contrast ratio. Our analysis show that the high contrast ratio is due to the high reflectivity from the second interface, where light is reflected at the solid core of LMA-PCF. In addition, we experimentally confirmed that two other parameters: the length of the sensing cavity and the offset for fusion splice the PCFs, can also affect the contrast ratio of the spectrum.

2. Sensor Principle and Fabrication

Fig. 1(a) shows the schematic diagram of the fiber-based gas pressure sensor. A section of long hollow-core silica capillary tube (SCT) with an air core of 75 μm in diameter (Model number: TSP005150) was fusion spliced between the SMF and a 3 mm long micro-structure fiber (MSF). The cross-section of the capillary tube with the same outer diameter of 125 μm is shown in Fig. 1(b). The capillary tube was the sensing cavity while the MSF with air holes acts as the gas inlet to the external environment. Light travels from SMF to the MSF, reflected twice at two separate interfaces "M1" "M2" due to refractive index mismatch. The reflectivities of M1 and M2 are given by Eqn. (1).

$$R_1 = \left(\frac{n_{core} - n_{air}}{n_{core} + n_{air}}\right)^2 R_2 = \left(\frac{n_{eff} - n_{air}}{n_{eff} + n_{air}}\right)^2 \quad (1)$$

where n_{core} and n_{air} represent for the refractive index of silica core and air, respectively. n_{eff} denote for the effective refractive index of the PCF with air-hole, which is determined by the microstructure of the fiber.

To prevent possible reflections from the end surface of MSF, we use a long piece of MSF up to a few millimeters such that the loss is high inside the MSF and reflections from the end surface can be neglected. Therefore, the reflected beam intensity of the proposed sensor is a result of a simplified interference model under the two-beam approximation [16]:

$$I = I_1 + I_2 + 2\sqrt{I_1 I_2}\cos\frac{2\times\pi\times\Delta}{\lambda} = I_1 + I_2 + 2\sqrt{I_1 I_2}\cos\frac{2\times\pi\times n_{air}\times L}{\lambda} \tag{2}$$

where I_1, I_2 represent the intensities of reflected beams from "M1" and "M2", λ is the optical wavelength, Δ is the optic path difference (OPD) of the two reflected beam, which is equal to the product of refractive index of air n_{air} and cavity length L. The wavelength of the interference dip λ_{m} can be described as the following equation when Δ is equal to $(2m+1)\pi$:

$$\lambda_m = \frac{4}{2m+1} n_{air} L_1 \tag{3}$$

The free spectral range (FSR) can be written as:

$$FSR = \frac{\lambda_m \times \lambda_{m+1}}{2n_{air}L_1} \approx \frac{\lambda^2}{2n_{air}L_1} \tag{4}$$

The refractive index(RI) of air n_{air} inside the sensing cavity is a function of pressure P (Pa) and temperature T(°C) :

$$n_{air} = 1 + \frac{2.8793\times10^{-9}\times P}{1+0.003671\times T} \tag{5}$$

At a constant temperature, the RI of air increases linearly as pressure increases. As a result, the wavelength of the interference dips will shift to longer wavelength according to Eqn (3). The sensitivity of this wavelength shift can be calculated by taking the derivative of λ_{m} with respect to gas pressure:

$$\begin{aligned} S = \frac{d\lambda_m}{dP} &= \frac{4}{2m+1} n_{air}\frac{dL_1}{dP} + \frac{4}{2m+1} L_1 \frac{dn_{air}}{dP} \\ &= \frac{\lambda}{L_1}\frac{dL_1}{dP} + \frac{\lambda}{n_{air}}\frac{dn_{air}}{dP} \approx \frac{\lambda}{n_{air}}\frac{dn_{air}}{dP} \end{aligned} \tag{6}$$

The sensitivity S is the sum of two terms. The first term represents the influence of pressure change on cavity length, while the second term is caused by the variation of RI of air due to pressure change. The first term is reported to be tens of pm/MPa [4], which is three orders of magnitude smaller than the second term, and thus can be neglected. Combined (3) with (6), the pressure sensitivity at 1500 nm is calculated to be 4.32 nm/MPa.

Using the hollow-core silica capillary as the sensing cavity, we investigated the role of gas inlets using different types of PCFs. Fig. 2(a–d) showed the microscopic pictures of pressure sensors S1–S4 with four different PCFs as gas inlets (Table 1), while Fig. 2(e–h) are the cross-sections of the PCFs corresponding to the four sensors. The bright and dark area represents silica and air holes, respectively. Among the four fibers, only the large mode area (LMA) PCF shown in Fig. 2(e) has a solid core. The mode field diameter is about 10 μm. The hollow-core MSF in S4 has a 10 μm hollow-core and a microstructure of 75 μm in diameter.

The senor is completed by splicing the silica capillary between the SMF and MSF using an arc fusion splicer (Fujikura FSM-80S). During the fabrication process, it is essential to obtain a smooth cleave surface and complete the fusion splice without collapsing the microstructure holes. Table 2 gives the sample fusion parameters of the two splices for S1. The length of the sensing cavity is about 247 μm for S1, corresponding to a FSR of about 4.6 nm at 1510 nm. The MSF serves as the gas inlet which is chosen to be 3 mm long to prevent possible reflections from the end surface.

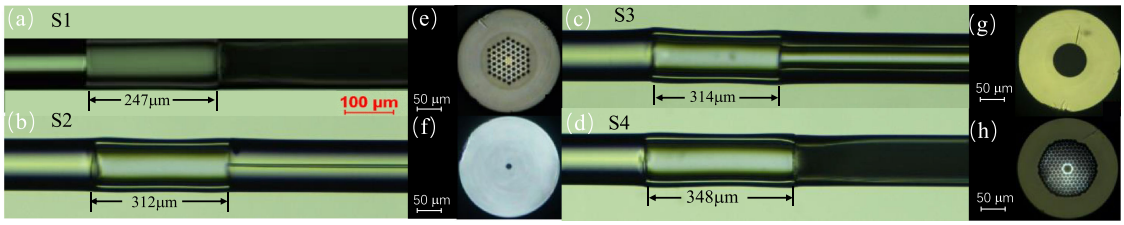

Fig. 2. (a–d) The side view of four pressure sensors. Fibers from left to right: SMF, 75 μm silica capillary (Fig. 1(b)), and PCFs as gas inlets. (e–f) The cross section of the four PCFs serving as gas inlets.

TABLE 1
Parameters for Four PCFs as the Gas Inlets

Sensor	Sensing cavity type	Gas inlet(fiber type)	Diameter of the hollow structure	Outer diameter
S1	75 μm capillary	Solid-core large-mode-area (LMA) PCF	10 μm	125 μm
S2	75 μm capillary	Hollow-core silica capillary	5 μm	125 μm
S3	75 μm capillary	Hollow-core silica capillary	40 μm	125 μm
S4	75 μm capillary	Hollow-core MSF	10 μm/75μm	125 μm

TABLE 2
Splicing Parameters for the Gas Pressure Sensor

	SMF-75 μm capillary	75 μm capillary-LMA PCF
Fiber end separation	10 μm	15 μm
Overlapping	10 μm	20 μm
Discharge intensity	-70 bit	-70 bit
Discharge time	500 ms	600 ms

3. Experiment and Discussion

Fig. 3 illustrated our experimental setup for gas pressure measurement. The sensor head was inserted into a vacuum chamber. The closed system was initially evacuated by a mechanical pump to a background pressure of 5×10^{-3} Pa. The pressure inside the chamber was increased by slowly introducing dry nitrogen gas. A vacuum gauge (ZJ-1Y, Cdreborn Electronics Co. Ltd) with a measurement range from 0.5 kPa-350 kPa was used to monitor the pressure reading. Light from a broadband source (BBS, YSL, 900–1700 nm) went through a circulator into the sensor. The reflected light went back to the circulator. The interference spectrum was observed in the optical spectrum analyzer (OSA, YOKOGAWA AQ6370B), with a maximum resolution of 0.02 nm.

3.1 Pressure Sensitivity

Fig. 4 shows the reflection spectrum from 1500 to 1520 nm for S1–S4 under a pressure of one atmosphere with OSA resolution of 0.02 nm. The fast Fourier Transform (FFT) analysis of S1 in Fig. 4(b) shows that the major peak at 0.2 nm^{-1} corresponding to a cavity length of 247 μm. This indicates that the main interference fringes in Fig. 4(a) are caused by the two reflection beams from interfaces M1 and M2. At the end surface of MSF, since the outside environment is air, light

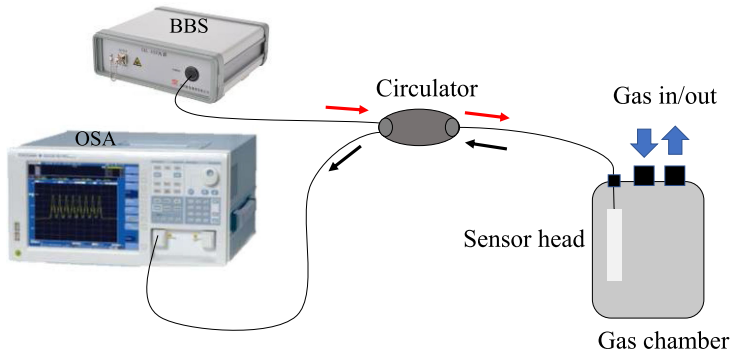

Fig. 3. Experimental apparatus for the gas pressure measurement.

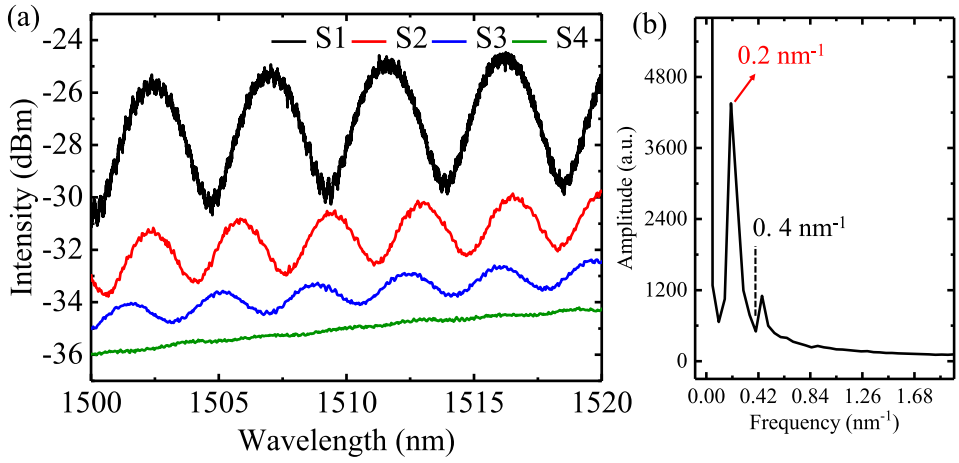

Fig. 4. (a) Reflection spectrum for S1-S4 at one atmosphere. (b) Fast Fourier Transform of the reflection spectrum for S1 (Black curve in (a)).S1.

travelling in glass will be reflected back to MSF due to refractive index mismatch. The reflected light at the end surface interfers with the reflection from M2, and can cause another high frequency oscillation on top of the main interference pattern. Further calculation confirms that the free spectral range of such oscillations in Fig. 4(a) matches the length of the MSF by Eqn FSR $= \lambda^2/2nL$, indicating that the high frequency oscillations are caused by reflections from the end surface of the MSF.

Among the four sensors, S1 has the highest contrast ratio of 5 dB while S4 has the smallest contrast ratio of 0.1 dB. In order to obtain a smooth reflection spectrum for pressure measurement, we filtered the high frequency components above 0.4 nm^{-1}. Fig. 5(a) shows an example of filtered spectrum for S1 under different pressures. We can observe that the interference dip experiences red shift as pressure increases from 22.3 kPa to 142 kPa. The linear fitting of the sensitivity is 4.27 nm/MPa, as shown in Fig. 5(b). Fig. 6 shows the sensitivities for S2 and S3 for comparison. The sensitivities are measured to be 3.62 nm/MPa, and 4.04 nm/MPa, respectively, with good linearity. These results agree with the calculated value of 4.32 nm/MPa within 16% based on the interference theory under two-beam approximation in Section 2. The discrepancy may be caused by measurement error. Our results show that although using different PCFs, this FPI configuration gives similar pressure sensitivities. For better sensitivity performance, one can employ a thin flexible diaphragm in the FPI design [21], [22] or Vernier effect by introducing a second cavity to achieve magnified sensitivities [23]–[26].

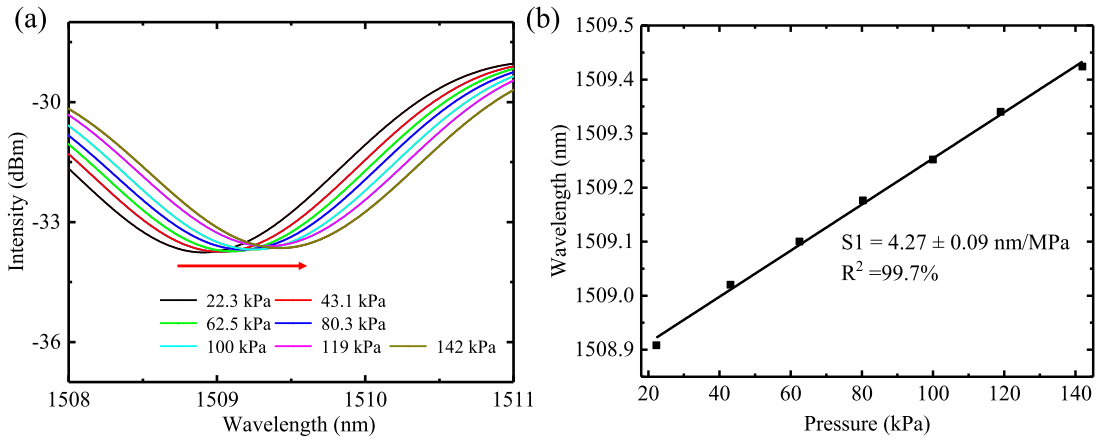

Fig. 5. (a) The reflection spectrum of S1under different pressure with high frequency components filtered above 0.4 nm^{-1}. (b) Linear fitting for the sensitivity.

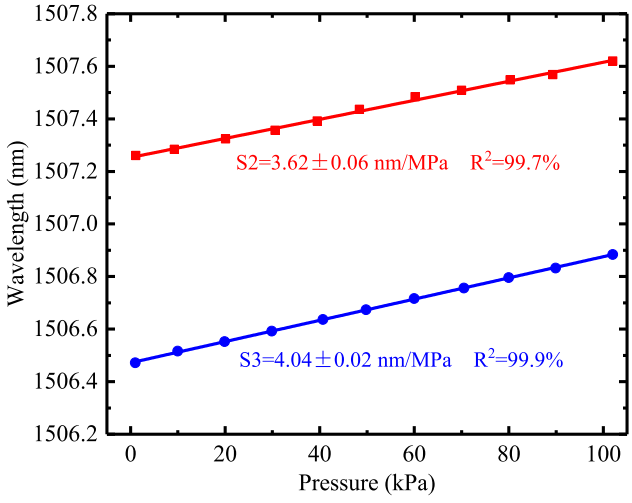

Fig. 6. Measured pressure sensitivity for S2 and S3 at around 1506 nm.

3.2 Contrast Ratio

Contrast ratio (CR) of the interference fringes is defined as the intensity difference between the maximum and minimum within a period. It is an important parameter for interferometer-based sensing applications. Our experimental results indicate that different types of PCF lead to different CR. In this section, we investigate how the microstructure of PCFs influence the contrast ratio. Our analysis show that the three factors contribute to an FP interference spectrum with high CR: the area of the solid surface where light can be reflected which determines the reflectivity of the two interfaces, the length of the sensing cavity, and the offset for splicing the PCFs.

In order to study how the microstructure of PCFs influence the contrast ratio, we simulated the mode field distribution of the PCFs. Fig. 7 shows the mode field profile of the electric field of the 5 μm silica capillary and the LMA-PCF. All simulation results are well converged. We choose these two fibers because the interference spectra of S1 and S2 have a larger contrast ratio than that of S3 and S4. When light travels to the interface M2 between the 75 μm silica capillary and the MSF, part of it will be reflected back. The reflectivity not only depends on the refractive index of both sides, but also on the physical structure of the MSF. The contrast ratio (CR) for an interference pattern

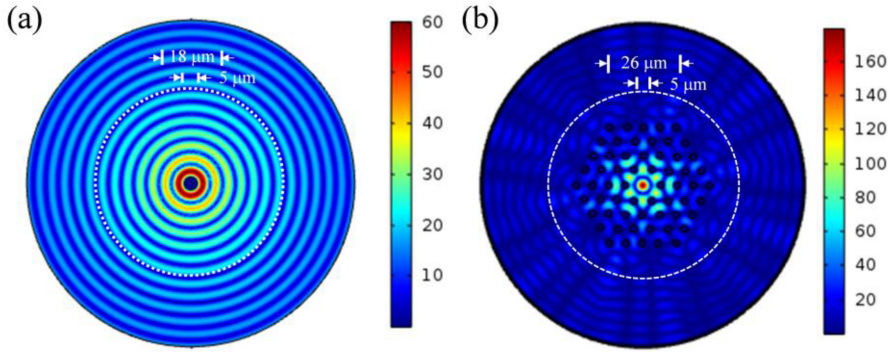

Fig. 7. Simulated modal field of (a) the capillary tube with hollow core diameter of 5 μm (S2), and (b) the large mode area photonic crystal fiber (S1) by Comsol. The white dashed circle represents a diameter of 75 μm.

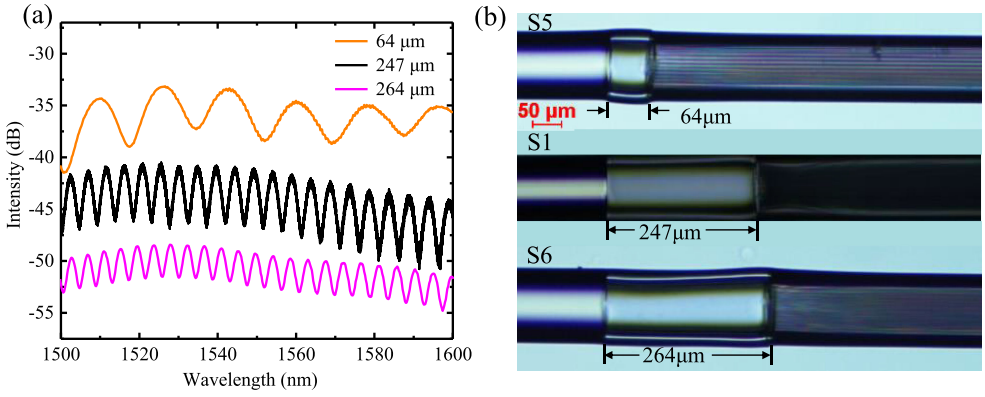

Fig. 8. (a) The optic reflection spectra of sensors with fiber types the same as S1 but different cavity lengths: 64 μm (orange), 247 μm (black) and 264 μm (pink). Intensity offsets are added for direct comparison. The length of LMA PCF is 3 mm. (b) Microscopic pictures of the corresponding sensors in (a).

can be evaluated quantitatively from the intensity of both beams involved in the interference by the following Eqn [15] :

$$CR = 10\log_{10}\left(\frac{1+\sqrt{I_2/I_1}}{1-\sqrt{I_2/I_1}}\right)^2 \tag{7}$$

With comparable intensities I_1 and I_2, high contrast ratio of interference fringes can be achieved. As seen from Fig. 7(a), the energy distribution for the 5 μm silica capillary is concentrated in a ring structure with 18 μm in diameter. Therefore, when light incidents on the 5 μm silica capillary, the majority of light will be reflected except the central air hole. In the solid-core LMA PCF as shown in Fig. 7(b), most energy is focused in the center indicating that when the beam incident on the second interface M2, most light will be reflected back to SMF and interfere with the first beam reflected by M1. However, in the case of S3 and S4, since the air-hole structure has a large diameter of 40 μm and 75 μm, a larger partial of light that incidents within this air hole area will be lost, resulting in a lower reflectivity for the second interface. Thus the CR is lower than S1 and S2, as shown in Fig. 4(a).

Besides the structure of PCF, the sensing cavity length is another factor that influences the CR. This is because the high optical loss for the silica capillary, which is measured to be 2.5 dB/mm. As the cavity length increases, the intensity of the incident beam on the second interface M2 will

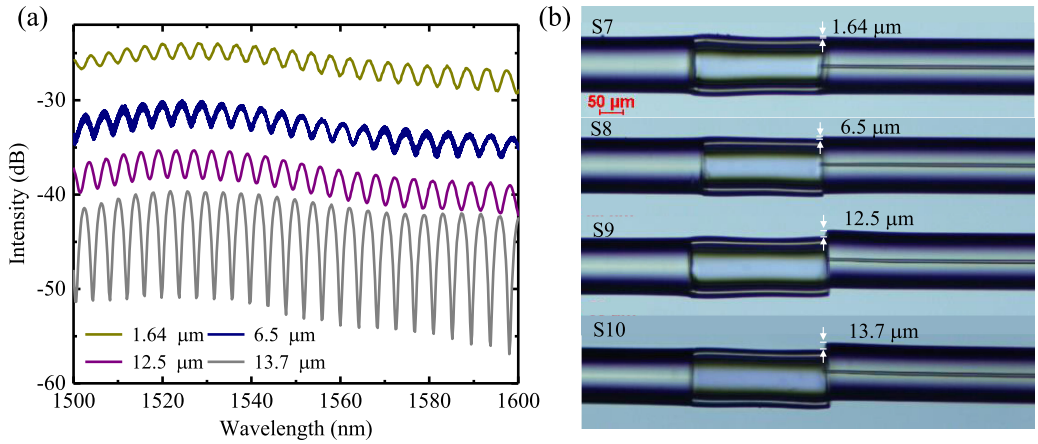

Fig. 9. (a) The optic reflection spectra of sensors with fiber types the same as S2, but different core-offsets: 1.64 μm (dark green), 6.5 μm (navy blue), 12.5 μm (purple) and 13.4 μm (grey). Intensity offsets are added for direct comparison. (b) Microscopic pictures of the corresponding sensors in (a).

become smaller. For a given reflectivity of M2, the reflected beam thus has a much lower intensity compared to the reflected beam at M1, which affects the interference performance. Fig. 8(a) shows the spectra of S1 with different sensing cavity lengths. When the cavity length is reduced from 264 μm to 64 μm, the CR increases rapidly from 3 dB to 7.1 dB at around 1510 nm. Our result shows the shorter cavity length gives higher CR.

In addition, we investigated how the CR can be improved by core-offset splicing the fiber through the fiber splicer. We fabricated four sensors with the same fiber type as S2, but with different core-offsets, which are S7, S8, S9 and S10. The CR of the fringes show dependence on the offset, as shown in Fig. 9. Fig. 9(a) shows a clear trend that the CR increases from 1.4 to 10.4 dB as the core-offset increase from $\sim$1.64 μm to $\sim$13.7 μm, however, at the expense of reduced robustness.

4. Conclusion

In summary, we systematically compare fiber-based gas pressure sensors in a Fabry-Perot configuration using different types of hollow-core photonic crystal fibers (PCFs). The sensing cavity consists of a segment of hollow-core silica capillary. Four types of PCFs were used to serve as the gas inlets for the sensors. We evaluated the pressure sensing performance for the four sensors. For the four sensors, the pressure sensitivities are measured to be 3.62$\sim$4.27 nm/MPa with a high linearity of 99.7% or above. These results are in good agreement with the calculated value of 4.32 nm/MPa based on the interference model under the two-beam approximation. Among the four different PCFs, the large-mode-area (LMA) PCF shows the highest fringe contrast in the reflection spectrum. The simulation for modal analysis reveals that LMA-PCF has a high reflectivity caused by the solid core. Furthermore, we experimentally verified that two other factors: the length of the sensing cavity, as well as the offset fusion splice, will influence the fringe contrast. By selecting an appropriate PCF, using short sensing cavities, and proper offset for fusion splice, one can achieve a high contrast ratio for real implementation. Pressure sensors in a Fabry-Perot configuration using PCFs have advantages of high sensitivity with good linearity, and ease of fabrication. They can potentially work in high-temperature environment. We believe that they are highly suitable for civil engineering, biochemical and many other important industrial areas.

References

[1] Y. Xu, Y. Zhao, J. Ren, Y. Zhang, and H. Peng, "An all-solid-state fiber-shaped aluminum–air battery with flexibility, stretchability, and high electrochemical performance," *Angewandte Chemie*, vol. 128, no. 28, pp. 8111–8114, 2016.

[2] M. Deng, C. P. Tang, T. Zhu, Y. J. Rao, and M. Han, "Refractive index measurement using photonic crystal fiber-based Fabry-Perot interferometer," *Appl. Opt.*, vol. 49, no. 9, pp. 1593–1598, 2010.
[3] D. J. J. Hu *et al.*, "Novel miniaturized Fabry–Perot refractometer based on a simplified hollow-core fiber with a hollow silica sphere tip," *IEEE Sensors J.*, vol. 12, no. 5, pp. 1239–1245, May 2011.
[4] J. Long, G. Bai-Ou, and W. Huifeng, "Sensitivity characteristics of Fabry-Perot pressure sensors based on hollow-core microstructured fibers," *J. Lightw. Technol.*, vol. 31, no. 15, pp. 2526–2532, Aug. 2013.
[5] R. Wang and X. Qiao, "Gas refractometer based on optical fiber extrinsic Fabry—Perot interferometer with open cavity," *IEEE Photon. Technol. Lett.*, vol. 27, no. 3, pp. 245–248, Feb. 2014.
[6] T. Jian *et al.*, "High-sensitivity gas pressure sensor based on Fabry–Pérot interferometer with a side-opened channel in hollow-core photonic bandgap fiber," *IEEE Photon. J.*, vol. 7, no. 6, Dec. 2015, Art. no. 6803307.
[7] Y. Yu, X. Chen, Q. Huang, C. Du, S. Ruan, and H. Wei, "Enhancing the pressure sensitivity of a Fabry–Perot interferometer using a simplified hollow-core photonic crystal fiber with a microchannel," *Appl. Phys. B*, vol. 120, no. 3, pp. 461–467, 2015.
[8] X. Zhong, Y. Wang, C. Liao, S. Liu, J. Tang, and Q. Wang, "Temperature-insensitivity gas pressure sensor based on inflated long period fiber grating inscribed in photonic crystal fiber," *Opt. Lett.*, vol. 40, no. 8, pp. 1791–1794, 2015.
[9] H. Liang *et al.*, "Diaphragm-free fiber-optic Fabry-Perot interferometric gas pressure sensor for high temperature application," *Sensors*, vol. 18, no. 4, pp. 1–11, 2018.
[10] Y. Jiang, Z. Fang, Y. Du, E. Lewis, G. Farrell, and P. Wang, "Highly sensitive temperature sensor using packaged optical microfiber coupler filled with liquids," *Opt. Exp.*, vol. 26, no. 1, pp. 356–366, 2018.
[11] Y. Li *et al.*, "High-performance fiber sensor via Mach-Zehnder interferometer based on immersing exposed-core microstructure fiber in oriented liquid crystals," *Opt. Exp.*, vol. 28, no. 3, pp. 3576–3586, 2020.
[12] Z. Xu *et al.*, "Investigation of temperature sensing characteristics in selectively infiltrated photonic crystal fiber," *Opt. Exp.*, vol. 24, no. 2, pp. 1699–1707, 2016.
[13] E. Reyes-Vera, C. M. Cordeiro, and P. Torres, "Highly sensitive temperature sensor using a sagnac loop interferometer based on a side-hole photonic crystal fiber filled with metal," *Appl. Opt.*, vol. 56, no. 2, pp. 156–162, 2017.
[14] M. Quan, J. Tian, and Y. Yao, "Ultra-high sensitivity Fabry–Perot interferometer gas refractive index fiber sensor based on photonic crystal fiber and vernier effect," *Opt. Lett.*, vol. 40, no. 21, pp. 4891–4894, 2015.
[15] B. Xu, C. Wang, D. Wang, Y. Liu, and Y. Li, "Fiber-tip gas pressure sensor based on dual capillaries," *Opt. Exp.*, vol. 23, no. 18, pp. 23484–23492, 2015.
[16] Y.-J. Rao, M. Deng, D.-W. Duan, and T. Zhu, "In-line fiber Fabry-Perot refractive-index tip sensor based on endlessly photonic crystal fiber," *Sensors Actuators A: Phys.*, vol. 148, no. 1, pp. 33–38, 2008.
[17] Z. Zhang *et al.*, "Diaphragm-free gas-pressure sensor probe based on hollow-core photonic bandgap fiber," *Opt. Lett.*, vol. 43, no. 13, pp. 3017–3020, 2018.
[18] Z. Zhang, J. He, B. Du, F. Zhang, K. Guo, and Y. Wang, "Measurement of high pressure and high temperature using a dual-cavity Fabry–Perot interferometer created in cascade hollow-core fibers," *Opt. Lett.*, vol. 43, no. 24, pp. 6009–6012, 2018.
[19] Z. Li, J. Tian, Y. Jiao, Y. Sun, and Y. Yao, "Simultaneous measurement of air pressure and temperature using fiber-optic cascaded Fabry–Perot interferometer," *IEEE Photon. J.*, vol. 11, no. 1, Feb. 2019, Art. no. 7100410.
[20] H. He, Y. Liu, Y. Liao, C. Lang, Y. Li, and S. Qu, "Simple fiber-optic sensor for simultaneous and sensitive measurement of high pressure and high temperature based on the silica capillary tube," *Opt. Exp.*, vol. 27, no. 18, pp. 25777–25788, 2019.
[21] J. Ma, W. Jin, H. L. Ho, and J. Y. Dai, "High-sensitivity fiber-tip pressure sensor with graphene diaphragm," *Opt. Lett.*, vol. 37, no. 13, pp. 2493–2495, 2012.
[22] Z. Zhang *et al.*, "High-sensitivity gas-pressure sensor based on fiber-tip PVC diaphragm Fabry–Pérot interferometer," *J. Lightw. Technol.*, vol. 35, no. 18, pp. 4067–4071, Sep. 2017.
[23] P. Chen, Y. Dai, D. Zhang, X. Wen, and M. Yang, "Cascaded-cavity Fabry-Perot interferometric gas pressure sensor based on vernier effect," *Sensors*, vol. 18, no. 11, pp. 1–11, 2018.
[24] L. Hongfeng, L. Fufei, G. Huiyong, and Y. Zhou and Dai, "Ultra-highly sensitive gas pressure sensor based on dual side-hole fiber interferometers with vernier effect," *Opt. Exp.*, vol. 26, no. 22, pp. 28763–28772, 2018.
[25] A. D. Gomes *et al.*, "Optical harmonic vernier effect: A new tool for high performance interferometric fibre sensors," *Sensors*, vol. 19, no. 6, pp. 1–19, 2019.
[26] Z. Li, Y. Zhang, W. Zhang, L. Kong, and B. Wang, "High-sensitivity gas pressure Fabry–Perot fiber probe with micro-channel based on vernier effect," *J. Lightw. Technol.*, vol. 37, no. 14, pp. 3444–3451, Jul. 15, 2019.